

# Entanglement Routing using Quantum Error Correction for Distillation

Ashlesha Patil\*, Michele Pacenti†, Bane Vasić†, Saikat Guha\* and Narayanan Rengaswamy†

\*Wyant College of Optical Sciences, University of Arizona, Tucson, AZ, USA

†Department of Electrical and Computer Engineering, University of Arizona, Tucson, AZ, USA  
{ashlesha, mpacenti, saikat, narayananr}@arizona.edu, vasic@ece.arizona.edu

**Abstract**—Bell-state measurement (BSM) on entangled states shared between quantum repeaters is the fundamental operation used to route entanglement in quantum networks. Performing BSMs on Werner states shared between repeaters leads to exponential decay in the fidelity of the end-to-end Werner state with the number of repeaters, necessitating entanglement distillation. Generally, entanglement routing protocols use *probabilistic* distillation techniques based on local operations and classical communication. In this work, we use quantum error correcting codes (QECCs) for *deterministic* entanglement distillation to route Werner states on a chain of repeaters. To maximize the end-to-end distillable entanglement, which depends on the number and fidelity of end-to-end Bell pairs, we utilize global link-state knowledge to determine the optimal policy for scheduling distillation and BSMs at the repeaters. We analyze the effect of the QECC’s properties on the entanglement rate and the number of quantum memories. We observe that low-rate codes produce high-fidelity end-to-end states owing to their excellent error-correcting capability, whereas high-rate codes yield a larger number of end-to-end states but of lower fidelity. The number of quantum memories used at repeaters increases with the code rate as well as the classical computation time of the QECC’s decoder.

**Index Terms**—Quantum networks, entanglement distillation, quantum error correction, entanglement routing

## I. INTRODUCTION

Shared entanglement over long distances can be used for entanglement-assisted sensing, distributed quantum computation, and quantum key distribution. Quantum networks aim to provide shared entanglement between remote parties. Special purpose nodes called *quantum repeaters* [1], are used to route entanglement in the network. The quantum repeaters store the qubits either in matter-based quantum memories [2], [3] or using quantum error-correcting codes on photonic graph states [4], [5], and can perform quantum circuits and measurements on the stored qubits.

In a typical entanglement routing protocol, shared entanglement is generated by creating Bell states between quantum

repeaters, followed by performing joint projective measurements, e.g., Bell state measurements (BSMs) [6] or GHZ projections [7], [8], on qubits of the entangled states at the repeaters. Entanglement routing protocols can be classified into two categories: those using ideal Bell states and those with noisy Bell states [9]. In this paper, we focus on designing routing protocols with the latter. We assume that the link-level entangled states generated between neighboring repeaters are Werner states, i.e., Bell states that have undergone depolarizing noise.

The fidelity of a Werner state decays exponentially with the number of BSMs it has undergone, making it eventually unusable when used for routing in quantum networks. As a result, the fidelity of Werner states in quantum networks must be boosted periodically. This is precisely the purpose of performing entanglement distillation, which consumes  $n \geq 2$  noisy Bell states to generate  $k \geq 1$  higher fidelity Bell states. Several quantum circuits have been proposed for entanglement distillation [10]–[13]. These circuit-based techniques implement local single- and two-qubit gates and single-qubit measurements at each node. The measurement results are communicated between the nodes to *herald* distillation, making these techniques probabilistic in nature. The probability of successful distillation is proportional to the fidelity of the input states.

Another approach to distill entangled states involves using quantum error correcting codes (QECC). For an  $[[n, k, d]]$  QECC,  $n$  noisy Bell states are first shared between Alice and Bob. One of them, say Alice, measures the QECC’s stabilizers on her  $n$  qubits and communicates the syndrome to Bob through a perfect classical communication channel. Then Bob performs error correction on his  $n$  qubits by measuring the same stabilizers and comparing the syndrome with Alice’s. Finally, both of them unencode their qubits to obtain  $k$  pairs of entangled qubits that are of higher fidelity due to error correction. The QECC-decoder pair determines the fidelity of the  $k$  output states. Although quantum circuit-based probabilistic distillation is seemingly different from QECC-based distillation, Bennett et al. [10] showed that these two methods are inter-convertible. Wilde et al. [14] first showed the use of convolutional codes for distillation. Rengaswamy et al. [15], [16] developed QECC-based distillation protocols for GHZ states.

Ref. [17] studies entanglement routing on a chain of re-

This work was co-funded by the National Science Foundation (NSF) ERC Center for Quantum Networks under grant number 1941583 and NSF grant number CIF-2106189. The work of Michele Pacenti and Bane Vasić is also supported by NSF under grants CIF-1855879, CCF-2100013 and ECCS/CCSS-2027844, and in part by Jet Propulsion Laboratory, California Institute of Technology, under a contract with the National Aeronautics and Space Administration and funded through JPL’s Strategic University Research Partnerships (SURP) program. Bane Vasić has disclosed an outside interest in his startup company Codelucida to The University of Arizona. Conflicts of interest resulting from this interest are being managed by The University of Arizona in accordance with its policies.

peaters using quantum low-density parity check (QLPDC) codes for trapped ion repeaters. It performs distillation between every pair of adjacent repeaters to calculate the number of end-to-end entangled states. In this work, we use quantum convolutional and toric codes for entanglement distillation along a chain of repeaters. We map the error correction code to an entanglement distillation protocol that always succeeds by translating the qubit error probability and the logical error rate of the code to infidelities of the input and output states for distillation, respectively. In our protocol, the generation of *links*, which are Werner states shared between adjacent repeaters, is probabilistic, while the Bell state measurements at the repeaters are deterministic. We assume that the quantum memories are perfect. Instead of distilling between every pair of repeaters, we have a dynamic scheduling of distillation, i.e., we decide which repeaters would perform distillation based on outcomes of link generation. We incorporate a central processor in our protocol that takes all repeaters' link outcomes as the input to determine the scheduling of distillations along the chain of repeaters. The scheduling uses the total distillable entanglement of the end-to-end states shared between Alice and Bob as the cost function. We show that the code rate determines the fidelity and the quantity of the end-to-end states. We also give the timing diagram of our protocol to calculate the latency, and use it to determine the quantum memory requirements as a function of the timescales of various protocol steps.

The paper is organized as follows: Section II reviews Werner states and quantum error-correcting codes (QECCs). Section III first describes the mapping of QECC to entanglement distillation, followed by the entanglement routing protocol. Section IV compares the entanglement rates and quantum memory requirements for three QECCs with different rates. We conclude by summarizing the main results and future work in Section V.

## II. BACKGROUND

### A. Werner states

When the Bell state  $|\Phi^+\rangle = \frac{|00\rangle + |11\rangle}{\sqrt{2}}$  is subjected to the depolarizing noise channel,  $\mathcal{N} : \rho \mapsto W \cdot \rho + \left(\frac{1-W}{4}\right) \cdot \mathbf{I}$ , it transforms into the mixed state

$$\rho_W = W |\Phi^+\rangle \langle \Phi^+| + \left(\frac{1-W}{4}\right) \mathbf{I}. \quad (1)$$

Here,  $\mathbf{I}$  is the identity operator,  $\rho_W$  is the Werner state, and  $W$  is called the Werner parameter. Since depolarizing noise probabilistically replaces the input state with the completely mixed state  $\mathbf{I}$ , it is information-theoretically the most difficult noise to correct, making it ideal to evaluate the worst-case performance of the distillation protocol. We can expand Eq. (1) in the Bell basis to obtain the equivalent expression

$$\rho_W = F |\Phi^+\rangle \langle \Phi^+| + \frac{1-F}{3} (|\Phi^-\rangle \langle \Phi^-| + |\Psi^+\rangle \langle \Psi^+| + |\Psi^-\rangle \langle \Psi^-|). \quad (2)$$

The fidelity of  $\rho_W$  w.r.t. the Bell state  $|\Phi^+\rangle$  is  $F = \frac{3W+1}{4}$ .

When a BSM is performed on two Werner states with fidelities  $F_1$  and  $F_2$ , if the quantum gates and the measurements are ideal, then the resulting state is also a Werner state with fidelity [9]

$$F = \frac{1}{4} + \frac{3}{4} \left(\frac{4F_1 - 1}{3}\right) \left(\frac{4F_2 - 1}{3}\right). \quad (3)$$

Equivalently, the Werner parameter of the final state is  $W = W_1 W_2$ . Note that  $F < F_1, F_2$  for  $F_1, F_2 < 1$ . For a chain of  $n$  repeaters, if each repeater performs BSM, then the fidelity of the final Werner state decays with  $n$  as.

$$F = \frac{1}{4} + \frac{3}{4} \prod_{i=1}^{n+1} \left(\frac{4F_i - 1}{3}\right). \quad (4)$$

$F_i$  is the fidelity of  $i$ -th link.

Distillable entanglement measures the amount of quantum information in a mixed state. It represents the number of perfect Bell states that can be distilled from infinite copies of the mixed state using local operations and classical communication (LOCC) [10], [18]. For a Werner state with fidelity  $F$ , the distillable entanglement is given by

$$D(F) = 1 + F \log_2 F + (1-F) \log_2 \frac{1-F}{3}. \quad (5)$$

It is useful to note that  $D(F) > 0$  only if  $F > 0.8107$ .

### B. Quantum error correction for entanglement distillation

1) *Stabilizer formalism*: Let  $I, X, Y$ , and  $Z$  denote the Pauli operators and  $\mathcal{G}_n$  denote the  $n$ -qubit Pauli group, which consists of Kronecker products of these operators along with global phases from  $\{\pm 1, \pm i\}$ , where  $i = \sqrt{-1}$ . Then a stabilizer group  $\mathcal{S}$  is defined as an Abelian subgroup of  $\mathcal{G}_n$  that does not contain  $-I$ . The stabilizer group  $\mathcal{S}$  is generated by a set of  $n - k$  independent generators. If  $k = 0$ , then  $\mathcal{S}$  is called a *maximal* stabilizer group, and its unique common  $+1$ -eigenstate is called a *stabilizer state*. When a Pauli measurement is applied to a stabilizer state, it is possible to apply the *stabilizer formalism* [19], [20] to update  $\mathcal{S}$  such that the resulting stabilizer group uniquely identifies the post-measurement state. The Bell state  $|\Phi_n^+\rangle_{AB} = |\Phi^+\rangle_{AB}^{\otimes n}$  is a stabilizer state, and its stabilizer group is  $\langle X_A X_B, Z_A Z_B \rangle^{\otimes n}$ . It can be shown that  $|\Phi_n^+\rangle_{AB}$  satisfies the *Bell state matrix identity* [10]:

$$(M_A \otimes I_B) |\Phi_n^+\rangle_{AB} = (I_A \otimes M_B^T) |\Phi_n^+\rangle_{AB}, \quad (6)$$

where  $M$  is an arbitrary  $n$  qubit operator. If  $M$  is a projector, i.e.,  $M^2 = M$ , then one can replace  $M$  by  $M^2$  and apply this property to only one  $M$  so that the operator on the right hand side becomes  $(M_A \otimes M_B^T)$ . This means that projecting Alice's qubits by  $M$  induces a simultaneous projection of Bob's qubits by  $M^T$ . If Alice's qubits are projected onto a stabilizer code via measurements of the stabilizers of the code, then Bob's qubits are also projected onto an equivalent "transpose" code, whose stabilizers are the transposed versions of Alice's stabilizers. Since  $Y^T = -Y$ , the transpose retains the Pauli stabilizers up to a phase factor of  $-1$ .

2) *Stabilizer codes*: An  $[[n, k, d]]$  stabilizer code is a  $2^k$ -dimensional subspace  $\mathcal{C}$  of the Hilbert space  $(\mathbb{C}^2)^{\otimes n}$  that satisfies the condition  $S|\Psi\rangle = |\Psi\rangle \forall S \in \mathcal{S}, |\Psi\rangle \in \mathcal{C}$ . The minimum distance  $d$  is defined as the minimum number of non-identity operators of an element of  $\mathcal{N}(\mathcal{S}) \setminus \mathcal{S}$ , where  $\mathcal{N}(\mathcal{S})$  is the normalizer of  $\mathcal{S}$  in  $\mathcal{G}_n$ . Each Pauli error  $E \in \mathcal{G}_n \setminus \mathcal{N}(\mathcal{S})$  corresponds to a non-trivial syndrome, i.e., a vector  $\mathbf{s} \in \{1, -1\}^{n-k}$  where the  $i$ -th entry is  $-1$  if and only if  $E$  anti-commutes with the  $i$ -th generator of  $\mathcal{S}$ . The syndrome is obtained as the result of measurements of the stabilizers of the code. By definition, if  $E \in \mathcal{N}(\mathcal{S})$ , then  $\mathbf{s} = \mathbf{1}$ . Given a non-trivial syndrome, a decoding algorithm takes the measured syndrome and the set of stabilizers as inputs, and outputs an estimate of the corresponding error,  $\hat{E}$ , that is consistent with the syndrome. Then, a *recovery* is attempted by applying the estimated error on the state. If the encoded logical state after the recovery is preserved, i.e., if  $\hat{E}E \in \mathcal{S}$ , then we say that the decoder succeeded; otherwise, if  $\hat{E}E \in \mathcal{N}(\mathcal{S}) \setminus \mathcal{S}$ , then we declare a *logical error*.

3) *The Toric code*: It is a  $[[2d^2, 2, d]]$  stabilizer code that can be described by a  $d \times d$  square lattice whose opposite boundaries are identified with each other (to make a torus). Here, qubits reside on edges and the set of stabilizers is given by the incidence relations between vertices, edges and faces [21]. Specifically, each face or plaquette (resp. vertex) represents a weight-4  $Z$ -type (resp.  $X$ -type) stabilizer acting on the four incident edges. It can be shown that the minimum distance of the code is indeed the lattice size,  $d$ . For decoding the toric code we consider the the minimum-weight perfect-matching (MWPM) decoder [22]. Since this algorithm has a high decoding latency, we also consider LILLIPUT [23], an efficient look-up table decoder for small toric codes.

4) *Quantum convolutional codes*: A quantum convolutional code (QCC) is defined by  $n - k$  commuting Pauli sequences  $S_0 = \{s_j, 1 \leq j \leq n - k\}$ , where  $s_j$  is of length  $(\nu + 1)n$  and  $\nu$  is called the *memory* of the code. The full stabilizer  $\mathbf{S}$  is infinite, which contains  $S_0$  as well as the shifts of  $S_0$  by multiples of  $n$  qubits, denoted as  $S_i, i \in \mathbb{N}$ . In this paper we consider the  $[[3, 1, 3]]$  QCC over  $\mathbb{F}_4$  from [24]. Its stabilizer matrix is the generator matrix of a classical rate-1/3 quaternary self-orthogonal convolutional code with memory  $\nu = 1$ , which is generated by the following generator as well as all its shifts by multiples of  $n = 3$  symbols:

$$s_1 = [1 \ 1 \ 1 \ 1 \ \omega \ \bar{\omega}]. \quad (7)$$

Note that  $\bar{\omega} = \omega^2$  in  $\text{GF}(4)$ . To perform the decoding, we use a quaternary syndrome Viterbi decoder [25].

5) *Entanglement distillation with error correction*: Quantum error correcting codes can be used to perform entanglement distillation [15]. Assume that Alice and Bob want to share high-fidelity Bell pairs, and that Alice can generate  $n$  Werner states (noisy Bell pairs), each with Werner parameter  $W$ . The  $2n$  qubits can be represented by the stabilizer group  $S_W(|\Phi_n^+\rangle_{AB})$ , which has  $2n$  generators. Alice projects her qubits onto the code space of an  $[[n, k, d]]$  stabilizer code by measuring the  $n - k$  stabilizer generators of the code and,

using the stabilizer formalism, updates the stabilizer group, i.e., the signs of stabilizers. The code  $\mathcal{Q}(\mathcal{S})$  is then defined by the set of stabilizers and the results of the measurements, which we still call *syndrome* even though they are random and do not arise from a Pauli error on the state. Due to (6), Bob's qubits will also be projected onto the "transpose" code, and his stabilizers must belong to the evolved group  $S'_W$ . In total, there will be  $2(n - k)$  code stabilizer generators for this group; the remaining  $2k$  operators are not stabilizers, but since they all commute with all the stabilizers (due to the evolution of the stabilizer group), they must be logical operators of Alice's and Bob's qubits. It is possible to conclude that those logical operators correspond to logical operators  $X_A X_B$  and  $Z_A Z_B$  for each of the  $k$  encoded Bell pairs (see [15] for more details).

After Alice projects her  $n$  halves of Werner states onto the code space, she can send Bob's qubits to him. Since we can see Werner states as perfect Bell pairs going through depolarizing noise, we can use (6) to consider Alice's qubits as perfect Bell pairs and Bob's qubits as affected by additional depolarizing noise. Alice then sends the qubits labeled with  $B$  to Bob, along with the syndrome of the stabilizer group after the evolution, which are sent through a classical channel. If the quantum channel is a depolarizing channel, then the additional Pauli errors will add on top of Bob's already corrupted qubits. Now, Bob measures all the stabilizer generators on his qubits; since the qubits are already projected onto  $\mathcal{Q}(\mathcal{S})$  from Alice's measurement, the outcome of Bob's measurement is an *error syndrome*, which he can use to correct errors using a decoder. If the amount of noise is correctable by the stabilizer code, and if the decoder succeeds, then Bob can revert the Pauli errors on his qubits, and the resulting state corresponds to  $k$  perfect Bell pairs shared between Alice and Bob, encoded in two  $[[n, k, d]]$  quantum stabilizer codes. Otherwise, if a logical (uncorrectable) error occurs, one or more of the encoded Bell states will be altered to one of the orthogonal Bell states. This protocol can further be extended to the case where the stabilizer code is a quantum convolutional code [14]. After performing the distillation, Alice and Bob can retrieve the  $k$  distilled Bell pairs by independently applying the inverse encoding circuit of the stabilizer code  $\mathcal{Q}(\mathcal{S})$  on their  $n$  physical qubits.

### III. THE GLOBAL LINK-STATE PROTOCOL

In this section, we discuss an entanglement routing protocol assuming the quantum memory coherence time is longer than all other timescales in the network. Hence, the wait times do not affect the quality of Werner states stored in quantum memories. We first discuss using QECCs for entanglement distillation, followed by the routing protocol and its latency.

#### A. Entanglement distillation

Section II-B5 discusses the use of  $[[n, k, d]]$  QECC to distill  $n$  Werner states into  $k$  Werner states. We now calculate the output fidelity and the success probability of this scheme.

Our paper utilizes the toric and quantum convolutional codes for entanglement distillation, and decoders (MWPM and

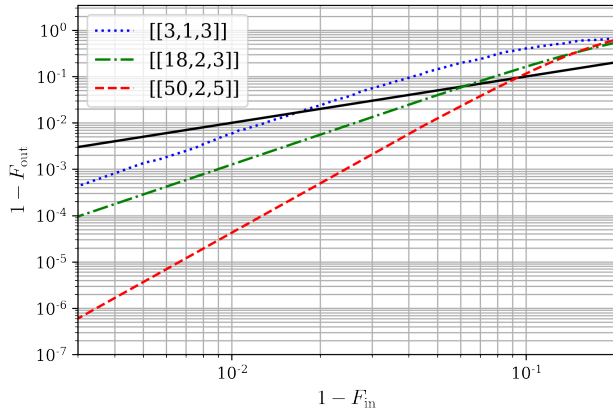


Fig. 1. The infidelity ( $1 - F_{\text{out}}$ ) of the output Werner state distilled using QEC codes vs. infidelity ( $1 - F_{\text{in}}$ ) of the input Werner state. The  $[[3, 1, 3]]$  code is a quantum convolutional code while the other two are toric codes.

Viterbi) that always converge to a valid error estimate. We then map the decoder’s convergence probability to the distillation success probability, resulting in a distillation success probability of 1 for the toric and quantum convolutional codes. However, the decoder’s convergence does not ensure a state free of uncorrectable errors, leading to logical errors in the output state. We map the logical error probability of the code to the infidelity of the output state(s) of distillation. Similarly, the infidelity of the input state is the error probability in the QECC. We relabel the logical error rate vs. qubit error probability plot for the  $[[n, k, d]]$  QECC with rate  $k/n$  as the output infidelity ( $1 - F_{\text{out}}$ ) vs. the input infidelity ( $1 - F_{\text{in}}$ ) as shown in Fig. 1. We assume that the syndrome measurements on the QECC are perfect. For a given quantum code, there exists a threshold fidelity  $F_{\text{th}}$  such that if  $F_{\text{in}} < F_{\text{th}}$ , then  $F_{\text{out}} < F_{\text{in}}$ , i.e., the quantum code fails to improve the input Werner state fidelity. We refer to  $F_{\text{th}}$  as the pseudo-threshold of the code.

### B. The protocol

We have a linear chain of  $N$  repeaters connecting users Alice and Bob at a distance  $L$  from each other. We assume that the quantum memories are perfect, i.e. their coherence times are much larger than all other timescales of the protocol.

In every time slot of length  $\tau$  seconds, each repeater generates  $2M$  Werner states and transmits  $M$  qubits from those states over the parallel optical channels on either side. The Werner states from adjacent repeaters meet at the *intermediate nodes* and undergo photonic BSM. Each BSM succeeds i.i.d. with probability  $p$ . The successful BSMs generate *links*, i.e., Werner states each with fidelity  $F_0$  between the quantum memories at each pair of neighboring repeaters. Here,  $M$  is the spatial multiplexing block length. The time required to generate links is  $\tau_l = \frac{L}{2(N+1)c_f}$ , where  $c_f$  is the speed of light in optical fiber.

The network’s link state after an attempt to generate links is called the *snapshot*. We use a *central processor* to incorporate global link-state knowledge. Once the links are generated,

the minor nodes send their link-state to the processor. The processor uses a brute-force method (see Section III-C) to devise a scheduling strategy for the received snapshot. We assume that the classical computation required to calculate the scheduling strategy is instantaneous. The scheduling strategy decides which repeaters perform distillation. We refer to those repeaters as the “distillation repeaters”; the remaining repeaters that perform only BSMs are called the “BSM repeaters”. The processor relays this strategy to all repeaters. It includes the operations at every repeater and their sequence until Alice and Bob are delivered entangled states.

We assume that it takes time  $\tau_p$  to send the snapshot to the processor and receive the scheduling strategy at all the repeaters. Assuming that the processor is located halfway between Alice and Bob, we have  $\tau_p = \frac{(2N+1)L}{2(N+1)c_f}$ .

For two sets of  $n$  links on opposite sides of a BSM repeater, the link-level BSMs at the repeater and the distillation at the neighboring repeaters do not commute. As a result, the distillation is performed after the BSMs at the BSM repeaters. We assume that the BSM is deterministic but takes time  $\tau_{\text{BSM}}$ . The BSM repeaters perform BSMs on the maximum number of possible links simultaneously.

The distillation repeaters perform distillation using an  $[[n, k, d]]$  QECC as discussed in Section III-A. Let  $\tau_{\text{Dec}}$  be the runtime of the classical decoder during distillation. We consider the decoding runtime of MWPM to be around  $1ms$  (see `qecsim` implementation [22]). In comparison, the runtime of an FPGA implementation of the Viterbi decoder is around  $1\mu s$  for a rate-1/3 convolutional code [26]. However, for the toric codes ( $n = 18$  and  $n = 50$ ), we consider efficient look-up tables that achieve a runtime lower than  $50ns$  [23].

Once the distillation is complete, every repeater communicates the Pauli corrections from distillation to the central processor, which then transmits all the corrections to Bob. This classical communication step takes time  $\tau_{\text{Dist}} = \frac{L}{c_f}$  (to communicate the distillation outcomes from Alice) and affects only the latency of the protocol. The distillation repeaters apply BSM on the distilled links to generate end-to-end Werner states between Alice and Bob. Links with the highest fidelity are paired together to perform BSM and maximize distillable entanglement. All repeaters send the BSM outcomes to Bob. The upper limit for the time required to send the BSM outcomes is the time it takes to send them from the repeater farthest from Bob, so  $\tau_{\text{CC}} = NL/((N+1)c_f)$ . Bob applies Pauli corrections to his qubits based on the distillation and BSM outcomes. We define entanglement rate as the sum of the distillable entanglement of all end-to-end Werner states ( $D_{\text{total}}$ ) per optical mode per time step  $\tau$ , i.e.,  $D_{\text{total}}/(2M\tau)$ . We assume that link qubits are encoded in the dual-rail photonic basis, resulting in two optical modes per qubit.

After the protocol starts, assuming  $\tau_{\text{BSM}} < \tau_{\text{Dist}} < (\tau_{\text{BSM}} + \tau_{\text{CC}})$ , Bob finishes applying Pauli corrections on the first end-to-end state at time  $\tau_{\text{lat}} = \tau_l + \tau_p + 2\tau_{\text{BSM}} + \tau_{\text{Dec}} + \tau_{\text{CC}}$ , the initial classical communication latency of the protocol as shown in Fig. 3.  $\tau_{\text{Dist}}$  does not affect the latency as the pauli

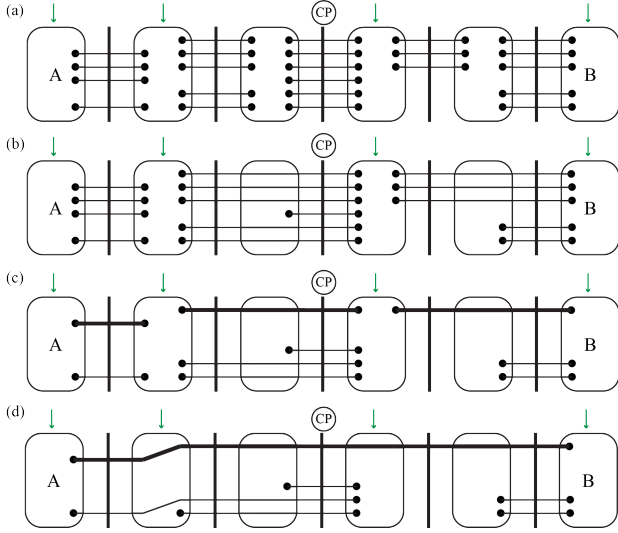


Fig. 2. Schematic of the protocol with  $M = 6$ ,  $n = 3$ , and  $k = 1$ . The central processor is shown as a circle halfway between Alice and Bob. (a) Snapshot of the network. Links (black lines) are generated between the neighboring repeaters' quantum memories (black circles). The vertical black lines are intermediate nodes used to generate links. The distillation repeaters are marked with green arrows; the remaining are the BSM repeaters. (b) The BSM repeaters perform BSM on all possible links. (c) The distillation repeaters then divide the links into groups of three to distill one link with higher fidelity (thick black line) (d) Distillation repeaters that are not Alice or Bob perform BSM to get an end-to-end link.

corrections due to distillation reach Bob before the corrections due to BSMs.

### C. Scheduling strategy

The processor uses a brute-force method to decide the sequence of BSMs and distillations at the repeaters. This method searches over all possible BSM and distillation sequences. We first calculate  $C(N + 1)$ , the set of all possible compositions of the integer  $(N + 1)$ . A composition is an ordered partition of an integer. For example, all possible compositions of 3 are  $(1, 1, 1)$ ,  $(1, 2)$ ,  $(2, 1)$ ,  $(3)$ . Composition decides the hop distance between repeaters that perform distillation.

For a composition  $c = (n_1, n_2, \dots, n_i)$  in  $C(N + 1)$ , the distillation is performed between Alice and the  $n_1$ -th repeater, the  $n_1$ -th and  $(n_1 + n_2)$ -th repeater, and so on; the remaining repeaters are BSM. The central processor calculates the end-to-end distillable entanglement for the composition  $c = (n_1, n_2, \dots, n_i) \in C(N + 1)$  as follows:

- 1) The processor first performs BSM on maximum possible links at the BSM repeaters (refer Fig. 2(b)).
- 2) Once the BSMs are complete, the distillation repeaters will have long-range links between them. The fidelities of these long-range links are lower than  $F_0$ . The processor distills the long-range links using the following rules (refer Fig. 2(c)):
  - If a distillation repeater has  $l$  successful links with its neighbor, it divides them into groups of  $n$  to distill using an  $[[n, k, d]]$  code. The distillation step converts  $n$  links into  $k$  links with higher fidelity.

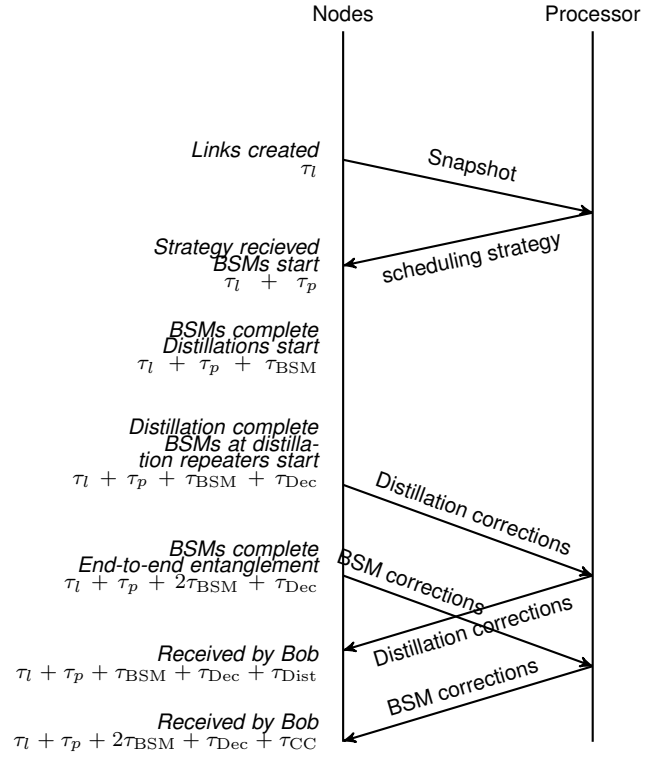


Fig. 3. Timing diagram to illustrate the latency of the protocol. Network nodes include Alice, Bob, and the repeaters. Here,  $\tau_{\text{BSM}} < \tau_{\text{Dist}} < (\tau_{\text{BSM}} + \tau_{\text{CC}})$ .

- The  $l \bmod n$  non-grouped links are not distilled.
  - The processor calculates the fidelity of links after BSMs using Eq.(4). It then decides to distill the links only if it improves the fidelity using Fig. 1.
- 3) Once the distillation is complete, at every distillation repeater, the processor pairs up their links (including the links that are not distilled) in the increasing order of fidelity to maximize the distillable entanglement and performs BSMs. This step creates end-to-end links between Alice and Bob (refer Fig. 2(d)).
  - 4) If the composition  $c$  generates  $m$  end-to-end link with fidelities  $F_i^c$ ,  $i \in \{1, 2, \dots, m\}$ , then the total distillable entanglement is  $D_{\text{total}}^c = \sum_{i=1}^m f(F_i^c)$  such that

$$f(F_i^c) = \begin{cases} D(F_i^c) & \text{if } F_i^c > 0.8107, \\ 0 & \text{otherwise.} \end{cases}$$

Here,  $D(F_i^c)$  is the distillable entanglement calculated using Eq. (5).

- 5) The processor calculates  $D_{\text{total}}^c$  for all compositions  $C(N + 1)$  and chooses the composition with the highest  $D_{\text{total}}^c$  to send to the repeaters. Maximizing  $D_{\text{total}}^c$  maximizes the number of shared Werner states while simultaneously ensuring that they are of high quality.

The steps above are performed on a classical computer at the processor. The repeaters perform measurements only according to the optimal composition, after receiving it from the processor.

## IV. RESULTS

### A. Rate calculations

In this section, we compare the performances of the  $[[3, 1, 3]]$  quantum convolutional code and the  $[[18, 2, 3]]$  and  $[[50, 2, 5]]$  toric codes for our global link-state protocol. We use the notation  $(n, N)$  for a protocol that uses  $[[n, k, d]]$  distillation code over a chain of  $N$  repeaters. Fig. 4(a) compares the three codes when  $F_0 = 0.99$ . The rate monotonically increases with the link success probability  $p$ , except for the  $(50, 8)$  protocol. The distillable entanglement for  $(50, 9)$  is much higher than  $(50, 8)$  for  $F_0 = 0.99$  and multiplexing  $M = 450$ . Fig. 4(b) shows the contributions of the number of end-to-end links and their average fidelity to the distillable entanglement when  $p = 1$ .

The optimal composition for the  $(50, 8)$  protocol is  $(1, 1, \dots, 1)$  for  $p = 1$ . This composition distills between every pair of repeaters as  $F_0$  exceeds the pseudo-threshold to generate  $M \times 2/50 = 18$  distilled links between adjacent repeaters. Consequently, Alice and Bob have 18 shared links.

On the other hand, the  $(10, 0)$  composition is optimal for the  $(50, 9)$  protocol, when  $p = 1$ . This composition first applies BSM at all repeaters to get  $M = 450$  long-range links (between Alice and Bob) with fidelity  $F'_{(10,0)}$ . For  $F_0 = 0.99$ ,  $F'_{(10,0)}$  falls below the pseudo-threshold of the  $[[50, 2, 5]]$  code; Alice and Bob do not distill the shared links. The result is  $M$  end-to-end links with fidelity  $F'_{(10,0)}$ .  $(1, 1, \dots, 1)$  is not the optimal composition as it generates only 18 links, although of higher fidelity than the  $(10, 0)$  composition. Our measurement strategy maximizes distillable entanglement, which depends on *both* the number and fidelity of states. The  $(10, 0)$  composition generates more links than  $(1, 1, \dots, 1)$ , compensating for lower quality links and resulting in a higher entanglement rate than the  $(50, 8)$  protocol. Similarly, the  $(3, 8)$ ,  $(3, 9)$ ,  $(18, 8)$ , and  $(18, 9)$  protocols perform only BSMs and no distillation, resulting in identical entanglement rates as the  $(50, 9)$  protocol. The entanglement rates for  $(3, 9)$  and  $(18, 9)$  are lower than  $(3, 9)$  and  $(18, 9)$  due to an additional BSM.

Note that, the  $(9, 0)$  composition for the  $(50, 8)$  protocol is not optimal. In this case, the fidelity of 450 links between Alice and Bob after BSMs at all repeaters is higher than pseudo-threshold, resulting in 18 distilled links between Alice and Bob, identical to the  $(1, 1, \dots, 1)$  composition. However, the fidelity of links is higher when the  $(1, 1, \dots, 1)$  composition is used.

The pseudo-threshold of the code, the input fidelity below which distillation does not improve the fidelity of the output states, plays a crucial role in determining the number and quality of the end-to-end states. The pseudo-threshold decreases with the code rate. Low-rate can distill input states with lower fidelity than high-rate codes. Moreover, a low-rate code consumes more links per distillation. As a result, using a low-rate code for distillation results in fewer but better quality end-to-end states than a high-rate code.

We use the same reasoning as above to explain a higher rate for  $p = 0.9$  than  $p = 1$  for the  $(50, 8)$  protocol. The

protocol generates more end-to-end states when  $p = 0.9$ , since, on average,  $pM$  links will be generated between repeaters. When  $p = 0.9$ , the links cannot be divided into perfect groups of 50. Ungrouped links will undergo only BSM, resulting in increased end-to-end links.

When we lower  $F_0$  to 0.97, the optimal composition for  $(18, 8)$ ,  $(18, 9)$ ,  $(50, 8)$ , and  $(50, 9)$  protocols is  $(1, 1, \dots, 1)$  (see Fig. 5). This results in a monotonic increase in the rate with  $p$  and  $F_{out}$  decreases with  $N$  for  $(18, 8)$ ,  $(18, 9)$ ,  $(50, 8)$ , and  $(50, 9)$  protocols.  $F_0 = 0.97$  is lower than pseudo-threshold of the  $[[3, 1, 3]]$  code, rendering this code unusable for distillation. In this case, the repeaters use the  $(N + 1, 0)$  composition. For the  $(N + 1, 0)$  composition when  $N = 8$  or  $N = 9$ , the fidelity of links between Alice and Bob after BSMs at all repeaters is lower than 0.8107, the threshold for non-zero distillable entanglement (see Eq.(5)), making the entanglement rate for the  $[[3, 1, 3]]$  code zero.

To summarize, for high  $p$ , the optimal compositions is:

- $(1, 1, \dots, 1)$  if the fidelity of links after all BSMs of the  $(N + 1, 0)$  composition is above the pseudo-threshold.
- $(N + 1, 0)$  if the fidelity of links after all BSMs in the  $(N + 1, 0)$  composition is below the pseudo-threshold. No distillation is performed.
- $(N + 1, 0)$  if  $F_0$  is below the pseudo-threshold.

### B. Quantum memory requirements

In this section, we calculate the upper bound to the number of quantum memories our protocol uses per repeater. The memories used per repeater depend upon the relative values of all the network timescales and the error correction code rate. We plot the number of quantum memories used as time progresses in Fig. 6 when  $p = 1$ . At time  $t = 0$ , a repeater starts link generation and utilizes  $2M$  memories. Every time step  $\tau$ , a repeater uses a new set of  $2M$  memories to store links. The number of quantum memories used at time  $t$  is  $2M(t/\tau + 1)$ . The BSM repeater frees  $2M$  memories for the first time by performing BSM at time  $\tau_l + \tau_p + \tau_{BSM}$  (refer Fig. 3). By this time, it has utilized  $2M[(\tau_l + \tau_p + \tau_{BSM})/\tau + 1]$  memories, assuming  $(\tau_l + \tau_p + \tau_{BSM})$  is a multiple of  $\tau$ . After the BSMs, the number of used memories reduces to  $2M(\tau_l + \tau_p + \tau_{BSM})/\tau$ . At time  $\tau_l + \tau_p + \tau_{BSM} + \tau$ , another  $2M$  memories are used, and the links generated at time  $t = 2\tau$  are measured. As a result, the maximum number of memories a BSM repeater uses is  $2M(\tau_l + \tau_p + \tau_{BSM})/\tau + 2M$ .

A distillation repeater accumulates memories until  $t = \tau_l + \tau_p + \tau_{BSM} + \tau_{Dec}$ , resulting in  $2M[(\tau_l + \tau_p + \tau_{BSM} + \tau_{Dec})/\tau + 1]$  used memories. Distillation reduces the number of used memories by  $2M(n - k)/n$ . The number of memories used increases until the distillation repeater finishes performing BSM on links generated at  $t = 0$ . The number of memories entangled at  $t = \tau_l + \tau_p + 2\tau_{BSM} + \tau_{Dec}$  are  $2M[(\tau_l + \tau_p + 2\tau_{BSM} + \tau_{Dec})/\tau + 1 - (1 + \tau_{BSM}/\tau)(n - k)/n]$ . They reduce to  $2M[(\tau_l + \tau_p + 2\tau_{BSM} + \tau_{Dec})/\tau - (\tau_{BSM}/\tau)(n - k)/n]$  after BSM on the  $k$  distilled links.

Note that, the distillation repeater requires more quantum memories than the BSM repeater due to the classical com-

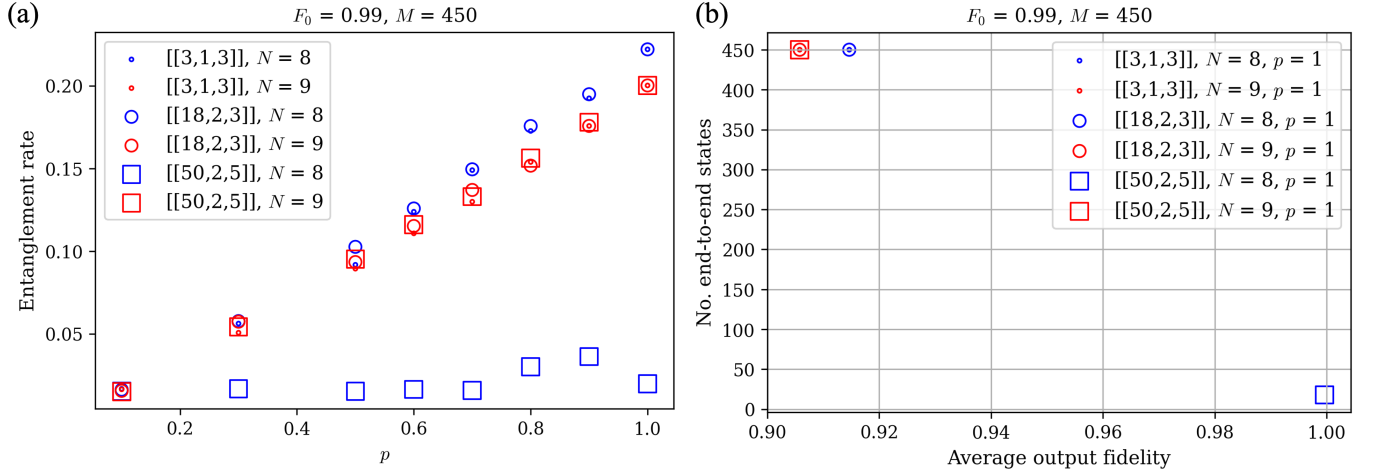


Fig. 4. Performance comparisons when the 18-qubit and 50-qubit surface codes are used for distillation. (a) Distillable entanglement as a function of  $p$  (b) Number of end-to-end states and the average fidelity of those states when  $p = 1$ .

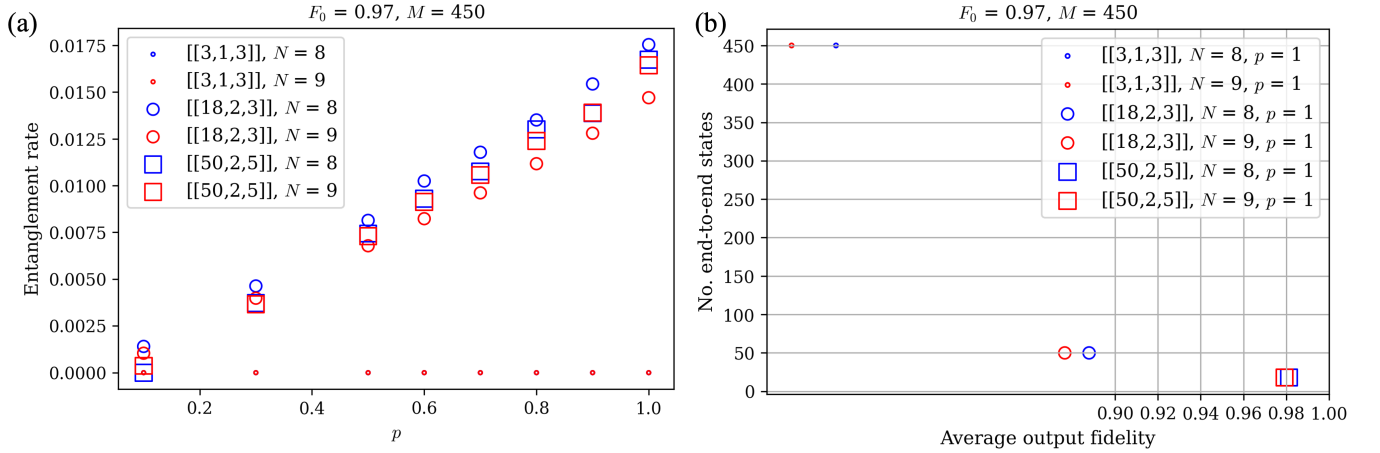


Fig. 5. Performance comparison for when the 18-qubit and 50-qubit surface codes are used for distillation. (a) Distillable entanglement as a function of  $p$  (b) Number of end-to-end states and the average fidelity of those states when  $p = 1$

putation time of decoding,  $\tau_{\text{Dec}}$ . If  $\tau_{\text{Dec}} \ll \tau$ , the BSM and the distillation repeaters would require the same number of memories. Similarly, increasing the code rate increases the maximum number of memories used at the distillation repeater.

## V. CONCLUSION AND DISCUSSION

We have designed a protocol to route Werner states on a chain of quantum repeaters. It utilizes quantum error-correcting codes (QECC) for entanglement distillation and global link-state knowledge to decide the location of distillation, if any, along the chain for maximum end-to-end distillable entanglement. We have designed a scheduling strategy for distillation that maximizes the end-to-end distillable entanglement for every network snapshot. The QECC's rate and pseudo-threshold determine the fidelity and number of end-to-end states between Alice and Bob. Lower code rates increase error-correction capability and result in higher output fidelity. Using a sufficiently low rate code allows the distribution of

long-range links with higher fidelity than shared links between repeaters at the start of the protocol. However, fewer end-to-end states are yielded as more links are consumed per distillation with decreasing code rates. These observations can help determine the code rate based on the specific application. A higher rate code is chosen for applications requiring many shared entangled states, while applications demanding high-quality links use a lower rate code. For low-rate code, multiplexing more increases the number of end-to-end links.

The code rate also dictates the number of quantum memories used at the distillation repeaters. In an  $[[n, k, d]]$  QECC, the fraction of freed quantum memories due to distillation is  $(n - k)/n$ . A low-rate code frees up more memories than a high-rate code, reducing memory requirements. The memory requirements grow with the classical computation time of the decoder. Reducing memory usage requires a low-rate code with a fast decoder.

In this work, we have assumed perfect quantum memories

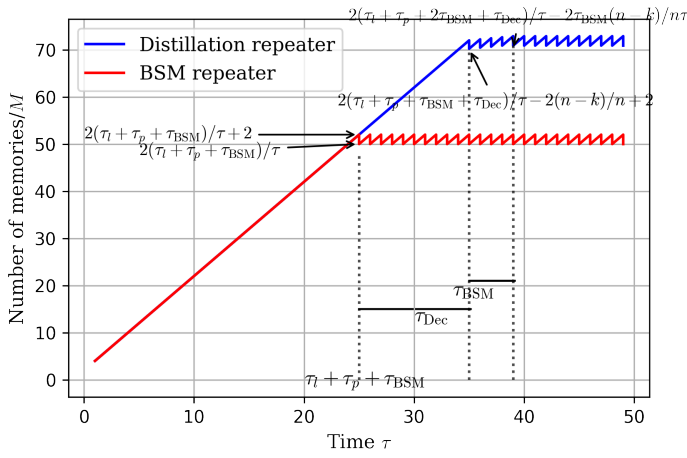


Fig. 6. The number of quantum memories used at distillation and BSM repeaters for the  $[[50, 2, 5]]$  code. Here,  $\tau_p = 20\tau$ ,  $\tau_l = \tau$ ,  $\tau_{\text{BSM}} = 4\tau$ ,  $\tau_{\text{Dec}} = 10\tau$ .

with infinite coherence times, s.t., the fidelity of links held in the memories does not degrade with time. A trivial protocol extension would incorporate quantum memories with finite coherence times. In this case, the links would decohere while waiting for classical communication, computation and BSM.

The optimal composition for the QECC codes used here is either  $(1, 1, \dots, 1)$  or  $(N + 1, 0)$ , depending upon the number of repeaters  $N$ , initial fidelity  $F_0$ , and the rate of the code. The  $(1, 1, \dots, 1)$  composition is optimal due to the deterministic distillation. We conjecture that if the distillation is probabilistic, i.e., if a penalty is associated with the distillation in the cost function to calculate the scheduling strategy, compositions with distillation between non-neighboring repeaters will become optimal. In future work, we aim to study our protocol with probabilistic QECC distillation techniques, such as in refs. [15], [17] and derive insights on the scheduling of distillation as a function of network parameters.

We have used global link state knowledge to design the scheduling strategy. We calculated the optimal compositions under different network parameters. This calculation makes it possible to schedule distillation using only local-link state knowledge for given network parameters. The local-link state protocol does not require a central processor to calculate the scheduling strategy. If a repeater knows their position along the chain,  $F_0$ , and the QECC used, it can locally decide if it is a distillation repeater. The local-link state protocol will have a reduced latency of  $2\tau_l + 2\tau_{\text{BSM}} + \tau_{\text{Dec}} + \tau_{\text{CC}}$ , and require  $2M(\tau_p - \tau_l)/\tau$  fewer quantum memories.

## REFERENCES

- [1] H.-J. Briegel, W. Dür, J. I. Cirac, and P. Zoller, “Quantum repeaters: the role of imperfect local operations in quantum communication,” *Physical Review Letters*, vol. 81, no. 26, p. 5932, 1998.
- [2] N. Sangouard, C. Simon, H. De Riedmatten, and N. Gisin, “Quantum repeaters based on atomic ensembles and linear optics,” *Reviews of Modern Physics*, vol. 83, no. 1, p. 33, 2011.
- [3] S. Guha, H. Krovi, C. A. Fuchs, Z. Dutton, J. A. Slater, C. Simon, and W. Tittel, “Rate-loss analysis of an efficient quantum repeater architecture,” *Physical Review A*, vol. 92, no. 2, p. 022357, 2015.
- [4] K. Azuma, K. Tamaki, and H.-K. Lo, “All-photonic quantum repeaters,” *Nature communications*, vol. 6, no. 1, p. 6787, 2015.
- [5] E. Kaur, A. Patil, and S. Guha, “Resource-efficient and loss-aware photonic graph state preparation using an array of quantum emitters, and application to all-photonic quantum repeaters,” *arXiv preprint arXiv:2402.00731*, 2024.
- [6] M. Pant, H. Krovi, D. Towsley, L. Tassiulas, L. Jiang, P. Basu, D. Englund, and S. Guha, “Routing entanglement in the quantum internet,” *npj Quantum Information*, vol. 5, no. 1, p. 25, 2019.
- [7] A. Patil, M. Pant, D. Englund, D. Towsley, and S. Guha, “Entanglement generation in a quantum network at distance-independent rate,” *arXiv preprint arXiv:2005.07247*, 2020.
- [8] A. Patil, J. I. Jacobson, E. Van Milligen, D. Towsley, and S. Guha, “Distance-independent entanglement generation in a quantum network using space-time multiplexed greenberger–horne–zeilinger (ghz) measurements,” in *2021 IEEE International Conference on Quantum Computing and Engineering (QCE)*. IEEE, 2021, pp. 334–345.
- [9] M. Victora, S. Tserkis, S. Krastanov, A. S. de la Cerda, S. Willis, and P. Narang, “Entanglement purification on quantum networks,” *Physical Review Research*, vol. 5, no. 3, p. 033171, 2023.
- [10] C. H. Bennett, D. P. DiVincenzo, J. A. Smolin, and W. K. Wootters, “Mixed-state entanglement and quantum error correction,” *Physical Review A*, vol. 54, no. 5, p. 3824, 1996.
- [11] S. Krastanov, V. V. Albert, and L. Jiang, “Optimized entanglement purification,” *Quantum*, vol. 3, p. 123, 2019.
- [12] D. Deutsch, A. Ekert, R. Jozsa, C. Macchiavello, S. Popescu, and A. Sanpera, “Quantum privacy amplification and the security of quantum cryptography over noisy channels,” *Physical review letters*, vol. 77, no. 13, p. 2818, 1996.
- [13] K. Goodenough, S. de Bone, V. L. Addala, S. Krastanov, S. Jansen, D. Gijswijt, and D. Elkouss, “Near-term  $n$  to  $k$  distillation protocols using graph codes,” *arXiv preprint arXiv:2303.11465*, 2023.
- [14] M. M. Wilde, H. Krovi, and T. A. Brun, “Convolutional entanglement distillation,” in *2010 IEEE International Symposium on Information Theory*, 2010, pp. 2657–2661.
- [15] N. Rengaswamy, N. Raveendran, A. Raina, and B. Vasić, “Entanglement purification with quantum LDPC codes and iterative decoding,” *Quantum*, vol. 8, 2024.
- [16] N. Rengaswamy, A. Raina, N. Raveendran, and B. Vasić, “Distilling ghz states using stabilizer codes,” *arXiv preprint arXiv:2109.06248*, 2021.
- [17] A. Kang, S. Guha, N. Rengaswamy, and K. P. Seshadreesan, “Trapped ion quantum repeaters with entanglement distillation based on quantum ldpc codes,” in *2023 IEEE International Conference on Quantum Computing and Engineering (QCE)*, vol. 1. IEEE, 2023, pp. 1165–1171.
- [18] W. Dür and H. J. Briegel, “Entanglement purification and quantum error correction,” *Reports on Progress in Physics*, vol. 70, no. 8, p. 1381, 2007.
- [19] D. Gottesman, “The heisenberg representation of quantum computers,” 1998.
- [20] A. Patil and S. Guha, “Clifford manipulations of stabilizer states: A graphical rule book for clifford unitaries and measurements on cluster states, and application to photonic quantum computing,” *arXiv preprint arXiv:2312.02377*, 2023.
- [21] E. Dennis, A. Kitaev, A. Landahl, and J. Preskill, “Topological quantum memory,” *Journal of Mathematical Physics*, vol. 43, no. 9, pp. 4452–4505, Aug. 2002.
- [22] D. K. Tuckett, “Tailoring surface codes: Improvements in quantum error correction with biased noise,” Ph.D. dissertation, University of Sydney, 2020, (qecsim: <https://github.com/qecsim/qecsim>).
- [23] P. Das, A. Locharla, and C. Jones, “Lilliput: a lightweight low-latency lookup-table decoder for near-term quantum error correction,” in *Proceedings of the 27th ACM International Conference on Architectural Support for Programming Languages and Operating Systems*, ser. ASPLOS ’22. New York, NY, USA: Association for Computing Machinery, 2022, p. 541–553.
- [24] G. D. Forney, M. Grassl, and S. Guha, “Convolutional and tail-biting quantum error-correcting codes,” *IEEE Transactions on Information Theory*, vol. 53, no. 3, pp. 865–880, 2007.
- [25] J. Schalkwijk and A. Vinck, “Syndrome decoding of convolutional codes,” *IEEE Transactions on Communications*, vol. 23, no. 7, pp. 789–792, 1975.

- [26] S. Y. Ameen, M. H. Al-Jammas, and A. S. Alenezi, "Fpga implementation of modified architecture for adaptive viterbi decoder," in *2011 Saudi International Electronics, Communications and Photonics Conference (SIEPC)*, 2011, pp. 1-9.